doi:10.1016/j.jmb.2007.05.065 J. Mol. Biol. (2007) 371, 256–268

JMB

Available online at www.sciencedirect.com

ScienceDirect

ELSEVIER

Spackling the Crack: Stabilizing Human Fibroblast Growth Factor-1 by Targeting the N and C terminus β-Strand Interactions

Vikash Kumar Dubey[1], Jihun Lee[2], Thayumana Somasundaram[3] Sachiko Blaber[1] and Michael Blaber[1]*

[1]*Department of Biomedical Sciences, Florida State University, Tallahassee FL 32306, USA*

[2]*Department of Chemistry and Biochemistry, Florida State University, Tallahassee FL 32306, USA*

[3]*Institute of Molecular Biophysics, Florida State University, Tallahassee FL 32306, USA*

**Corresponding author*

The β-trefoil protein human fibroblast growth factor-1 (FGF-1) is made up of a six-stranded antiparallel β-barrel closed off on one end by three β-hairpins, thus exhibiting a 3-fold axis of structural symmetry. The N and C terminus β-strands hydrogen bond to each other and their interaction is postulated from both NMR and X-ray structure data to be important in folding and stability. Specific mutations within the adjacent N and C terminus β-strands of FGF-1 are shown to provide a substantial increase in stability. This increase is largely correlated with an increased folding rate constant, and with a smaller but significant decrease in the unfolding rate constant. A series of stabilizing mutations are subsequently combined and result in a doubling of the ΔG value of unfolding. When taken in the context of previous studies of stabilizing mutations, the results indicate that although FGF-1 is known for generally poor thermal stability, the β-trefoil architecture appears capable of substantial thermal stability. Targeting stabilizing mutations within the N and C terminus β-strand interactions of a β-barrel architecture may be a generally useful approach to increase protein stability. Such stabilized mutations of FGF-1 are shown to exhibit significant increases in effective mitogenic potency, and may prove useful as "second generation" forms of FGF-1 for application in angiogenic therapy.

Keywords: FGF-1; β-barrel; stability; folding; unfolding

Introduction

Human fibroblast growth factor-1 (FGF-1) is a potent human mitogen for a variety of cell types including vascular endothelial cells, and can stimulate such cells to develop neo-vasculature capable of relieving ischemia. For this reason, FGF-1 is an angiogenic factor with applicability in "angiogenic therapy".[1–3] FGF-1 belongs to the β-trefoil superfold, characterized by a pseudo-3-fold axis of structural symmetry with the repeating motif being a pair of antiparallel β-strands (known as the "β-trefoil fold").[4,5] These three repeating structural motifs comprise a total of 12 β-strands that associate to form a six-stranded β-barrel capped at one end by three β-hairpins (forming the "β-trefoil" superfold; Figure 1). Residue positions 13–17 (using the 140 amino acid form of FGF-1 numbering scheme) of the N termini (β-strand I), and 131–135 of the C termini (β-strand XII), hydrogen bond with each other as a pair of antiparallel β-strands within the six-stranded β-barrel (juxtaposing the N and C terminus). When considering the 3-fold symmetry of the overall architecture, the N and C terminus are structurally related to two β-hairpin turns at positions 49–52 and 90–93 (Figure 1). Thus, the termini in the native structure represent a break in the main chain continuity that forms the β-barrel.

Quenched-flow hydrogen exchange in conjunction with multi-dimensional NMR spectroscopy has shown that the N and C terminus β-strand hydro-

Present address: V. K. Dubey, Department of Biotechnology, Indian Institute of Technology, Guwahati-781039, Assam, India.

Abbreviations used: FGF-1, human fibroblast growth factor-1; GuHCl, guanidine hydrochloride; FGFR, FGF receptor.

E-mail address of the corresponding author: michael.blaber@med.fsu.edu

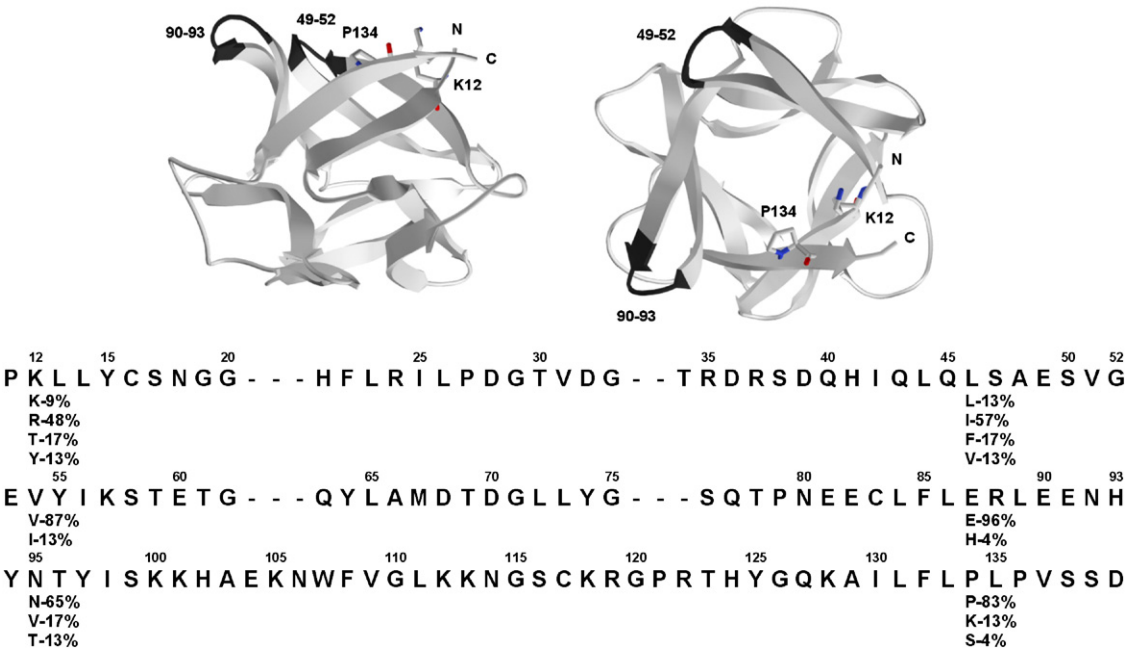

Figure 1. Upper panel: a ribbon diagram of FGF-1[23] showing the location of positions Lys12 and Pro134. The view on the right is looking down the β-barrel axis. Also shown are the turn regions (residues 49–52 and 90–93) related to the N and C-terminus by the pseudo-3-fold axis of symmetry inherent in the β-trefoil architecture. Lower panel: the primary structure of FGF-1 aligned to indicate the structural relationship of the three β-trefoil sub-domains. The statistics of the consensus residues at positions 12, 134 and symmetry-related positions for the 23-member FGF family of proteins are indicated.

gen-bonding interaction (i.e. β-strands I and XII, respectively) are the first to form in the folding pathway of FGF-1.[6] An analysis of correlated anisotropic thermal factors in a 1.10 Å atom-resolution X-ray structure of FGF-1, has identified the N and C terminus β-strands as demarcating a boundary of domain motion within FGF-1.[7] In the solution NMR structure of FGF-1 the interaction between β-strands I and XII becomes poorly defined and highly variable as one gets closer to the N and C terminus.[8] Thus, the structural data suggest that the N and C terminus β-sheet may represent a structurally weak region in the protein architecture, and this interaction may play an important role in folding and stability.

In an effort to study further the contribution of the N and C terminus β-strand interaction to the stability and folding of FGF-1, Cys mutations were introduced into each β-strand, near the termini, with the intention of linking them through a disulfide bond. In this case, stability and folding studies under oxidizing and reducing conditions would elucidate the contribution of the N and C terminus β-sheet formation to these processes. Two potential sites for such pair-wise mutations were identified at positions 12 and 134, and 13 and 135, respectively. These two pair-wise Cys mutations were constructed and initial stability studies were performed under oxidizing conditions. The Cys13/Cys135 mutation exhibited a substantial decrease in stability and was not pursued further. In contrast, the Cys12/Cys134 mutation exhibited a substantial increase in stability, suggesting that the introduced disulfide bond had stabilized the structure. However, repeating the stability studies under reducing conditions resulted in a further gain in stability. Therefore, the increase in stability for the Cys12/Cys134 mutation was due to the substitution of the wild-type Lys12 and/or Pro134 by Cys and not to disulfide bond formation.

Isothermal equilibrium denaturation, folding and unfolding kinetics, and X-ray structural studies have been utilized in characterizing the effects of Cys, Thr and Val mutations at positions 12 and 134 in FGF-1. The results show that substantial increases in stability can be achieved. However, native state structural changes appear quite modest and do not appear to entirely account for the observed improvements in stability; thus, destabilization of the denatured state cannot be excluded as an additional contributor to the observed stability increase.

Val mutations at the symmetry-related positions of residues 12 and 134 were also studied. A combined mutation, involving Val mutations at five positions, and introducing a 3-fold symmetric constraint at two positions within the FGF-1 structure, results in an increase in stability that doubles the original value of the ΔG of unfolding. This result suggests that although FGF-1 is known for generally poor stability the underlying β-trefoil architecture appears capable of extreme thermal stability. A combined mutation with enhanced stability also exhibits a 30-fold increase in mitogenic

potency and may prove useful as a "second generation" form of FGF-1 in angiogenic therapy.

Results

Mutant protein purification

All mutant proteins, except those containing Glu87Val, purified with high yield (~65 mg/l). Proteins containing the Glu87Val mutation appeared to have a lower solubility, resulting in some precipitation during purification and with somewhat lower yield (~35–40 mg/l).

Isothermal equilibrium denaturation

The thermodynamic parameters for the FGF-1 mutations are listed in Table 1. The standard error of ΔG from multiple analyses is approximately 1.0kJ/mol (0.24kcal/mol), which is also the typical magnitude of the standard deviation of the fit to the two-state model (data not shown). Thus, mutational effects upon stability can be reliably measured for values greater than 1kJ/mol, consistent with previous reports.

The substitution of Lys12 by Cys, Thr or Val provides an increase in stability of between −8.1 to −9.3 kJ/mol (Table 1). The highest midpoint of denaturation is observed for the Val mutation (1.53 M); however, overall, the Cys and Val mutations appear to be approximately equivalent in stability, with Thr slightly less so. The substitution of Pro134 by Cys, Thr or Val provides an increase in stability of between −6.1 to −8.8 kJ/mol. The highest midpoint of denaturation is observed for the Val mutation (1.49 M); Thr and Cys mutations are similar in magnitude, but again, slightly less stable than Val at this position. Combining Val mutations at positions 12 and 134 results in a −19.1 kJ/mol increase in stability. The simple sum of the individual point mutations predicts an increase in stability of −18.1 kJ/mol; thus, the effect of the combined mutations is essentially additive.

The Asn95Val mutation was constructed in the Lys12Val mutation background. Position 95 is related to position 12 by the 3-fold pseudo-symmetry inherent in the FGF-1 architecture (Figure 1). In reference to the Lys12Val mutation, the Asn95Val mutation stabilizes the protein by −6.4 kJ/mol, a magnitude similar to that of the Lys12Val mutation.

Individual Leu46Val and Glu85Val mutations were constructed in the Pro134Val mutation background to produce two double mutations. Positions 46 and 87 are related to position 134 by the 3-fold pseudo-symmetry in the FGF-1 architecture (Figure 1). In reference to the Pro134Val mutation, the Leu46Val mutation destabilizes the protein by a modest +1.2 kJ/mol, while the Glu87Val mutation is essentially neutral with regard to effect upon stability (Table 1). Combined Leu46Val and Glu87Val mutations were constructed in the Pro134Val mutation background. A simple sum of the individual mutational effects predicts an overall increase in stability of −7.1 kJ/mol in comparison to the WT* protein, and the actual combination mutation exhibits an increase in stability of −8.3 kJ/mol; thus, the effect upon stability for these combined mutations is essentially additive.

Finally, the Lys12Val and Asn95Val mutations (which constrain symmetry-related positions 12, 54 and 95 to Val) and Leu46Val, Glu87Val and Pro134Val mutations (which similarly constrain these symmetry-related positions to Val) were

Table 1. Thermodynamic parameters for FGF-1 mutations derived from isothermal equilibrium denaturation studies in ADA buffer

Mutation	ΔG[a] (kJ/mol)	*m*-value (kJ/mol M)	C_m (M)	$\Delta\Delta G$[b] (kJ/mol)
WT*	21.0	20.1	1.05	
Lys12Cys/Pro134Cys (reduced)	36.2±0.5	19.6±0.3	1.85±0.01	−15.9
Lys12Cys/Pro134Cys (oxidized)	30.5±0.7	18.3±0.4	1.67±0.01	−11.9
Lys12Cys	29.2±0.7	19.4±0.6	1.51±0.01	−9.1
Lys12Thr	26.2±0.9	17.8±0.6	1.47±0.02	−8.1
Lys12Val	27.7±0.5	18.1±0.3	1.53±0.01	−9.3
Pro134Cys	26.9±0.7	19.1±0.5	1.41±0.01	−7.1
Pro134Thr	26.9±0.4	19.9±0.3	1.35±0.01	−6.1
Pro134Val	28.8±0.7	19.3±0.5	1.49±0.01	−8.8
Lys12Val/Pro134Val	37.6±0.6	18.5±0.3	2.03±0.01	−19.1
Lys12Val/Asn95Val	34.1±1.0	18.3±0.6	1.86±0.02	−15.7
Leu46Val/Pro134Val	27.7±0.7	19.4±0.5	1.43±0.02	−7.6
Glu87Val/Pro134Val	27.7±0.9	18.8±0.6	1.47±0.02	−8.3
Leu46Val/Glu87Val/Pro134Val	28.8±1.3	18.7±0.8	1.54±0.02	−9.6
Lys12Val/Leu46Val/Glu87Val/Asn95Val/Pro134Val	40.6±1.3	16.6±0.6	2.45±0.02	−25.7

WT*, reference protein for all studies is the FGF-1 Cys117Val mutation[25] (see the text).

[a] ΔG value extrapolated to 0 M denaturant.

[b] $\Delta\Delta G = (C_{mWT^*} - C_{m\ mutation})(m_{WT^*} + m_{mutation})/2$, as described by Pace and Scholtz;[48] a negative value of $\Delta\Delta G$ indicates a more stable mutation. Error is the standard deviation of multiple data sets.

Table 2. Folding and unfolding kinetic parameters for WT* and mutation FGF-1 proteins

Mutation	k_f (s^{-1})	m_f (kJ/mol M)	k_u (1×10^{-3} s^{-1})	m_u (kJ/mol M)	m-value[a] (kJ/mol M)	C_m[b] (M)	$\Delta\Delta G$[c] (kJ/mol)	$\Delta\Delta G_F$[d] (kJ/mol)	$\Delta\Delta G_U$[e] (kJ/mol)	β_T[f]
WT*	3.28	−17.4	0.87	1.14	18.5	1.10	–	–	–	0.94
Lys12Cys	29.1±9.3	−17.4±0.8	0.29±0.09	1.68±0.2	19.1	1.50	−7.5	−5.4	2.8	0.91
Lys12Thr	53.6±11.7	−16.0±0.5	0.63±0.12	1.21±0.1	17.2	1.64	−9.5	−6.9	0.8	0.93
Lys12Val	43.0±16.4	−15.4±0.33	0.56±0.15	1.36±0.2	16.8	1.66	−9.9	−6.4	1.1	0.92
Pro134Cys	29.1±9.4	−16.9±0.7	0.41±0.05	1.39±0.1	18.3	1.51	−7.5	−7.3	1.9	0.92
Pro134Thr	9.62±2.2	−15.9±0.6	0.38±0.07	1.39±0.1	17.3	1.45	−6.3	−4.7	2.1	0.92
Pro134Val	10.1±1.00	−13.3±0.2	0.08±0.01	2.30±0.1	15.6	1.86	−13.0	−8.6	5.8	0.85
Lys12Val/Pro134Val	125±39	−15.0±0.5	0.09±0.02	2.13±0.1	17.2	2.04	−16.8	−14.7	5.6	0.88
Lys12Val/Asn95Val	161±31	−17.0±0.4	0.15±0.02	2.63±0.1	19.7	1.75	−12.4	−14.0	4.4	0.87
Leu46Val/Pro134Val	10.4±0.96	−15.9±0.2	0.54±0.04	1.51±0.1	17.4	1.40	−5.4	−4.1	1.2	0.91
Leu46Val/Glu87Val/Pro134Val	34.9±5.6	−16.7±0.3	0.71±0.05	1.41±0.1	18.1	1.48	−6.9	−6.4	0.5	0.92
Lys12Val/Leu46Val/Glu87Val/Asn95Val/Pro134Val	1678±513	−13.9±0.4	0.15±0.02	2.53±0.1	16.4	2.45	−23.6	−19.8	4.3	0.85

WT*, reference protein for all studies is the FGF-1 Cys117Val mutation[25] (see the text).
[a] (equation (6)).
[b] (equation (5)).
[c] (equation (2)).
[d] (equation (7)).
[e] (equation (8)).
[f] (equation (9)).

combined into a quintuple Val mutation. The summation of the individual stability effects of these five mutations predicts an overall increase in stability of −22.8 kJ/mol. The actual combination mutation exhibits an increase in stability of −24.1 kJ/mol (Table 1); therefore, the mutational effects are essentially additive.

Folding and unfolding kinetics

The results of the folding and unfolding kinetic analyses are listed in Table 2. As reported,[9] FGF-1 exhibits biphasic folding at low denaturant concentrations (<0.6 M guanidine hydrochloride (GuHCl)) that contributes to a characteristic "rollover" of the folding arm of the "chevron plot". Because of this, the ΔG m-values derived from the kinetic analyses are slightly lower than those measured by isothermal equilibrium denaturation, and correspondingly, the denaturation midpoint C_m values derived from the kinetics studies are shifted to slightly higher denaturant concentrations. This results in an approximate 5% disagreement in C_m and m-value thermodynamic parameters between the two methods, but overall the kinetic and thermodynamic analyses are in very good agreement (Tables 1 and 2).

The Cys, Thr, and Val point mutations at position 12 stabilize the protein primarily by increasing the folding rate constant (16 to 10-fold), with comparatively less-significant (1.4 to 3.0-fold) reduction in the unfolding rate constant. These changes in the folding and unfolding rate constants are associated with minimal changes in either the folding or unfolding kinetics "m values" (i.e. m_u, m_f). The effects of the Cys, Thr, and Val point mutations at position 134 upon the folding and unfolding rate constants are similar to the position 12 effects, in that the folding rate constant increases and the unfolding rate constant decreases; however, in this case the decrease in the unfolding rate constant (2.1 to 10.9-fold) is similar in magnitude to the increase in the folding rate constant (2.9 to 8.9-fold). Furthermore, the Val mutation at position 134 exhibits a twofold increase in the unfolding kinetics m value (i.e. increasing the cooperativity of unfolding; Table 2 and Figure 2) which is not observed in either the Cys or Thr mutation at this position, or in the position 12 point mutations (Table 2).

The various combination mutations, in each case, are more stable than the WT* protein and exhibit both an increase in folding rate constant, and

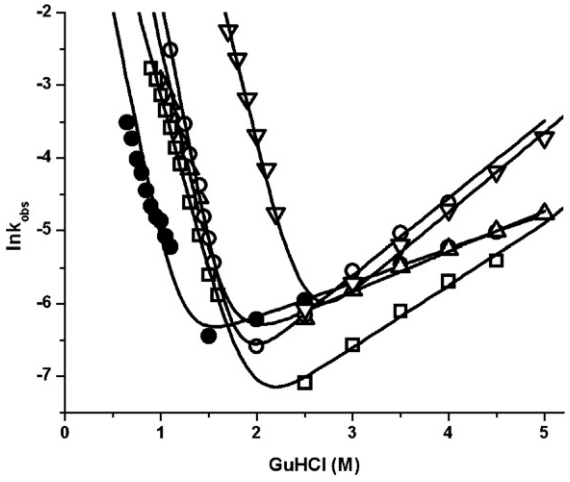

Figure 2. Folding and unfolding kinetics chevron plot for WT* (●), Lys12Val (△), Pro134Val (□), Lys12Val/Asn95Val (○), and Lys12Val/Leu46Val/Glu87→Val/Asn95Val/Pro134Val (▽).

decrease in unfolding rate constant. The effects upon folding and unfolding rate constants for the Lys12-Val/Pro134Val double mutation can be predicted from the contribution of the individual point mutations. The predicted increase in folding rate constant is 40.4-fold, with the observed increase being 38.1-fold; the predicted decrease in unfolding rate constant is 16.9-fold, with the observed decrease being 9.7-fold. Similarly, in the case of the final quintuple mutation, the effects upon folding and unfolding rate constants can be predicted from the contribution of the Lys12Val/Pro134Val double mutation and the Leu46Val/Glu87Val/Pro134Val triple mutation. The predicted increase in folding rate constant is 522-fold, with the observed increase being 512-fold; the predicted decrease in unfolding rate constant is 7.1-fold, with the observed decrease being 5.8-fold. Therefore, as observed for the effects upon stability, the effects upon folding and unfolding rate constants for the combination mutations essentially reflect the independent contributions of the constituent point mutations.

X-ray structures

Diffraction-quality crystals were obtained for the Lys12Cys, Lys12Val, Lys12Thr, Lys12Val/Asn95Val and Pro134Cys mutations (the majority of the position 134 mutations proving to be refractory to crystallization). All structures were refined to acceptable crystallographic residual and stereochemistry. Crystallographic data collection and refinement statistics for the mutations are listed in Table 3. All mutations, except Pro134Cys, crystallized in the WT* orthorhombic space group ($C222_1$) with two molecules in asymmetric unit. The Pro134Cys mutation crystallized in a novel monoclinic $P2_1$ space group with four molecules in the asymmetric unit. These four molecules were successfully positioned using the molecular replacement method and WT* FGF-1 as the search model. The $2F_o–F_c$ difference electron density was unambiguous at the mutation site(s), and the mutation structures could be modeled accurately in each case.

Mitogenic activity

The mitogenic activity (EC_{50}) for representative FGF-1 mutations is summarized in Table 4 (the WT* Cys117Val reference protein is essentially identical to wild-type FGF-1 in terms of stability, folding and mitogenic activity). The Cys and Val mutations at position 12 are approximately equivalent to each other in terms of mitogenic activity, and both are approximately 15 times more potent than WT* FGF-1. In contrast, while the Cys and Val mutations at position 134 are similarly equivalent to each other in terms of mitogenic potential, they exhibit only a modest increase in mitogenic activity compared to WT* (Table 4). The combination Val mutation at

Table 3. Crystallographic data collection and refinement statistics

	Lys12Cys	Lys12Val	Lys12Thr	Lys12Val/Asn95Val	Pro134Cys
Crystal data					
Space group	$C222_1$	$C222_1$	$C222_1$	$C222_1$	$P2_1$
Cell constants (Å)	$a=75.6$ $b=96.2$ $c=107.8$	$a=74.7$ $b=96.4$ $c=108.0$	$a=74.5$ $b=97.0$ $c=108.5$	$a=76.3$ $b=95.4$ $c=107.3$	$a=60.6$ $b=108.3$ $c=60.9$ $\beta=105.0°$
Max resolution (Å)	1.60	1.60	1.65	1.70	2.50
Mosaicity (°)	0.48	0.60	0.66	0.40	0.55
Mol/ASU	2	2	2	2	4
Matthews coeff. (Å/Da)	2.97	2.94	2.97	2.96	1.46
Data collection and processing					
Reflections total	452,889	480,263	396,717	384,008	127,309
Reflections unique	51,442	51,447	44,572	42,546	25,003
I/σ overall	39.9	45.0	37.2	44.8	13.6
I/σ highest shell	3.0	3.3	6.4	3.8	2.94
R_{merge} overall (%)	8.3	6.5	8.3	7.6	9.6
R_{merge} highest shell (%)	40.3	43.3	45.5	41.2	28.2
Completion overall (%)	99.6	97.3	97.6	99.8	98.0
Completion highest shell (%)	97.9	99.6	94.4	99.6	95.3
Refinement					
Non-hydrogen protein atoms	2532	2552	2501	2528	4598
Solvent molecules/ion	248	272	227	236	342
R_{cryst} (%)	20.0	18.8	23.2	19.7	17.3
R_{free} (%)	22.1	22.2	25.9	22.6	22.9
R.M.S.D. bond length (Å)	0.013	0.011	0.014	0.012	0.007
R.M.S.D. bond angle (°)	1.63	1.56	1.71	1.57	1.32
Ramachandran plot					
Most favored (%)	90.8	91.2	92.5	90.4	86.9
Additional allowed (%)	8.8	8.3	6.6	8.8	12.5
Generously allowed (%)	0.4	0.4	0.9	0.9	0.6
Disallowed region (%)	0.0	0.0	0.0	0.0	0.0
PDB accession codes	2HW9	2HWM	2HWA	2HZ9	2NTD

Table 4. Mitogenic activity of mutation FGF-1 proteins against NIH 3T3 fibroblasts

Protein	EC_{50}(ng/ml)
WT*	60.0±6.7
Lys12Cys	3.8±1.9
Lys12Val	4.2±1.7
Pro134Cys	50.4±7.6
Pro134Val	46.8±6.7
Lys12Val/Pro134Val	1.8±0.9
Lys12Val/Asn95Val	4,530±48
Leu46Val/Pro134Val	81.7±6.9
Glu87Val/Pro134Val	138±13
Lys12Val/Leu46Val/ Glu87Val/Asn95Val/Pro134Val	(No activity)

positions 12 and 134 appears to be largely additive, exhibiting an approximately 30-fold increase in mitogenic activity compared to WT*.

The Val mutation at position 95 exhibits a substantial ~1000-fold reduction in mitogenic activity. The Val mutations at positions 46 and 87 are associated with relatively minor reductions in mitogenic activity, with position 46 slightly less active than WT*, and position 87 exhibiting a twofold reduction in mitogenic activity. The combined Val mutation at positions 12, 46, 87, 95 and 134 exhibits no detectable mitogenic activity at concentrations up to 10^4 ng/ml, with higher protein concentrations observed to be toxic to 3T3 fibroblasts.

Discussion

Wild-type FGF-1 has previously been shown to exhibit two-state denaturation, with excellent agreement between the derived thermodynamic parameters as determined by isothermal equilibrium denaturation (monitored by fluorescence and circular dichroism) and differential scanning calorimetry.[9] Here, a comparison of the mutational effects upon overall protein stability ($\Delta\Delta G_{N\text{-}D}$ or $\Delta\Delta G$) as determined by both isothermal equilibrium denaturation and folding kinetics exhibits very good agreement (Figure 3, left panel). Kinetic analysis permits the mutational effects upon overall stability ($\Delta\Delta G$) to be compared to the individual changes in the free energy difference between native and transition states ($\Delta\Delta G_{N\text{-}\neq}$ or $\Delta\Delta G_U$) as well as transition and denatured states ($\Delta\Delta G_{D\text{-}\neq}$ or $\Delta\Delta G_F$). A comparison of these values shows that a significant proportion of the increased stability for the mutations correlates with $\Delta\Delta G_F$ (Figure 3, right panel). In other words, the observed increase in protein stability is largely correlated with reduction in the energetic barrier between the transition and denatured states, resulting in an increase in the folding kinetic constant. This change in energetics is relative, and is therefore due to either stabilization of the transition state, destabilization of the denatured state, or some combination thereof.

The contribution of $\Delta\Delta G_U$ to the observed increase in stability is lower in magnitude in comparison to the $\Delta\Delta G_F$ values, and exhibits less correlation with the overall stability change (Figure 3, right panel). This lower magnitude for $\Delta\Delta G_U$ suggests a greater correlation between native state and transition state energetics in contrast to that observed between transition and denatured states. The β_T value analysis of the kinetic data provides information regarding the solvent accessibility of the transition state;[10] a value close to 1.0 for β_T indicates a transition state that is native-like with respect to solvent-accessible surface area, and lower values indicate a transition state that is more like the unfolded state. The β_T values are near-unity for most of the mutations, but decrease slightly (0.85–0.88) for the Pro134Val, Lys12Val/Pro134Val double mutation, Lys12Val/Asn95Val double mutation, and the quintuple combination mutation (Table 2). Thus, the transition state solvent accessibility is essentially native-like for most mutations, with a slight shift towards the denatured-like accessibility for the above-mentioned mutations. Phi value analysis, using Cys point mutations as the reference (data not shown), indicates a $\Phi_{folding}$ value of 0.7 for both positions 12 and 134 (where a value of 1.0 indicates the position is as folded in the transition state as it is in the native state). Thus, the above analysis suggests that the transition state energetics largely correlate with the native state, albeit with modest relative stabilization of the native state (≤ ~5 kJ/mol; Figure 3, right panel).

Structural changes affecting the energetics of the native state in response to mutation can be eva-

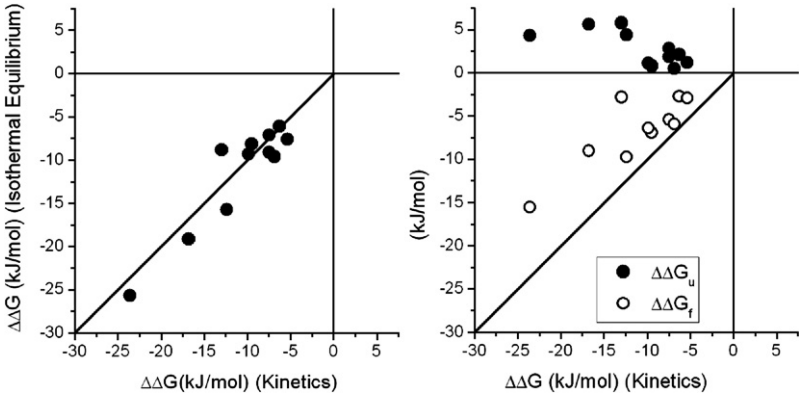

Figure 3. Left panel: a comparison of the $\Delta\Delta G$ values for the mutational effects upon FGF-1 stability derived from the folding and unfolding kinetic data (abscissa) and isothermal equilibrium denaturation data (ordinate). Right panel: a comparison of the mutation $\Delta\Delta G_U$ values (filled circles) and $\Delta\Delta G_F$ values (open circles) with the isothermal equilibrium $\Delta\Delta G$ values (ordinate).

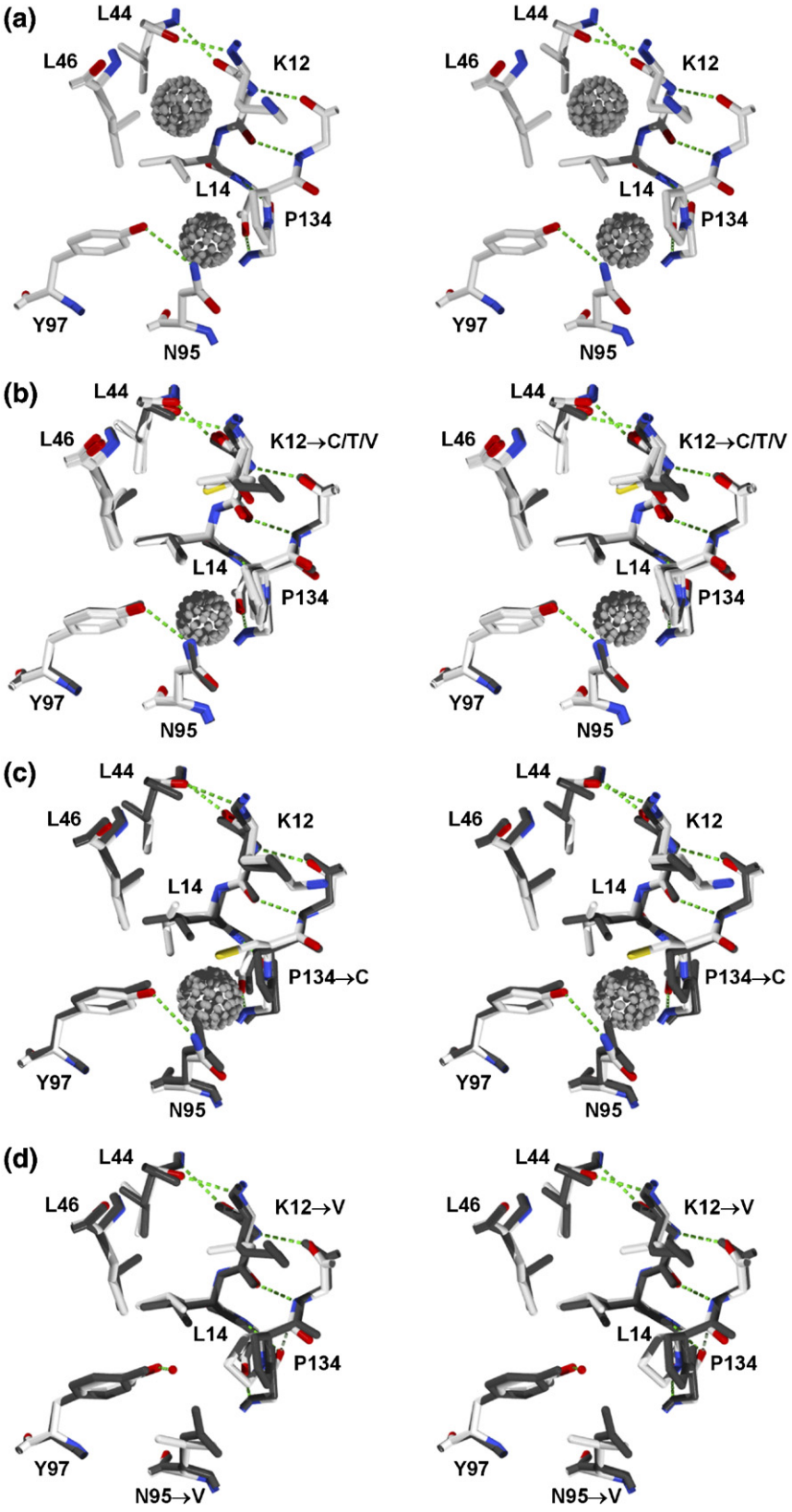

Figure 4. (a) Relaxed stereo diagram of the local structure of FGF-1 in the region of positions Lys12 and Pro134 and including the hydrogen-bonding network. Also shown are two small solvent excluded cavities, detectable using a 1.2 Å radius probe. (b) Relaxed stereo diagram showing an overlay of the Lys12Cys, Lys12Thr, and Lys12-Val X-ray structures with WT* (dark grey) in the region of the mutation site. The solvent excluded cavity adjacent to position 12 is filled with each mutation. (c) Relaxed stereo diagram showing an overlay of the Pro134Cys X-ray structure with WT* (dark grey) in the region of the mutation site. The solvent excluded cavity adjacent to position 12 is no longer detectable due to the rotation of the Leu14 side-chain. (d) Relaxed stereo diagram showing an overlay of the Lys12Val/Asn95Val X-ray structure with WT* (dark grey) in the region of the mutation site. The solvent excluded cavities adjacent to position 12 and 134 are no longer detectable due to the position 12 mutation and the adjustment of Pro134 in response to the position 95 mutation.

luated from the high-resolution X-ray diffraction data. X-ray structures were obtained for five mutations in the study: Lys12Cys, Lys12Thr, Lys12-Val, Pro134Cys, and Lys12Val/Asn95Val. The X-ray structure of FGF-1 exhibits two small solvent-excluded cavities (detectable using a 1.2 Å radius probe) in the region of residues 12, 95 and 134, each with a volume of approximately 9 $Å^3$ (Figure 4(a)). These cavities, which reside in the general interface between the N and C terminus β-strands, appear

partially filled in the X-ray structures of the point mutations (Figure 4(b) and (c)). The structure of the Lys12Val/Asn95Val double mutation indicates that these cavities are no longer detected (Figure 4(d)). Other than these relatively minor cavity-filling effects, no other significant structural alterations are apparent when comparing the available mutation and WT* structures. Filling a cavity within a protein should contribute 0.10–0.14 kJ/mol Å^3,[11] and therefore, filling each of these cavities should contribute a modest 0.9–1.3 kJ/mol towards improved protein stability ($\Delta\Delta G$).

The mutations in this study, in each case, were constructed within β-sheet secondary structure. Several β-sheet propensity scales, describing the intrinsic energetic differences between amino acids within β-sheet secondary structure, have been reported.[12–18] Presumably due to its being an imino acid, β-sheet propensity values for Pro are absent from β-sheet propensity tables, however, other all other residues can be directly compared. Substitution of Lys by either Cys, Thr, or Val is predicted to stabilize the structure by −1.6, −4.0, and −2.3 kJ/mol, respectively.[14] These mutations fill one of the two small cavities adjacent to position 12, which (as discussed above) would be expected to contribute an additional ~1.0 kJ/mol in stability. Thus, combining the mutational contributions of the intrinsic β-sheet propensity changes, plus cavity filling, suggests that the Lys12Cys mutation should stabilize the protein by −2.6 kJ/mol, the Lys12Thr mutation by −5.0 kJ/mol, and the Lys12Val mutation by −3.3 kJ/mol. The actual increases in stability for the Cys, Thr and Val mutations at position 12 are −9.1, −8.1, and −9.3 kJ/mol, respectively (Table 1), or significantly higher than the above predicted values.

Substitution of Asn by Val is predicted to stabilize the protein by −1.8 kJ/mol due to the change in β-sheet propensity.[14] Assuming that the Lys12Val/Asn95Val double mutation fills both local cavities, and taking into account the β-sheet propensity change for both residues, this double mutation is predicted to stabilize the structure by −6.4 kJ/mol. The actual increase in stability for this double mutation is −15.7 kJ/mol (Table 1), again, significantly higher than the predicted value.

Val mutations at positions Leu46 and Glu87 are accommodated with either neutral (+0.5kJ/mol; position 87) or slight destabilization effects (+1.2 kJ/mol; position 46). Both residue positions exhibit partial solvent accessibility, with the aliphatic region of both side-chains participating in van der Waals interactions with several adjacent hydrophobic residues. To a first approximation, substitution by Val would be expected to diminish these van der Waals interactions by the loss of a methyl group. Loss of a buried methyl group (~15 Å^3) is expected to destabilize the structure by ~ +2.0 kJ/mol. From β-sheet propensity changes, substitution of Leu by Val is predicted to stabilize the structure by −2.1 kJ/mol; similarly, substitution of Glu by Val is predicted to stabilize the structure by −3.0 kJ/mol. These calculations therefore predict an approximately equivalent energetic tradeoff between stability gain due to β-sheet propensity changes and stability loss due to loss of buried side-chain volume, in reasonably good agreement with the observed experimental values (i.e. essentially neutral mutational effects at these two positions).

β-Sheet propensity values are known to be highly context-dependent[14,16,19]; furthermore, there may be additional energetic contributions due to structural strain in the native state. However, analysis of the wild-type structure of FGF-1[7] indicates that Lys12 is present in a near-optimal *gauche*+ ($\chi1 = -60°$) rotamer orientation. Asn95 is similarly present in a *gauche*+rotamer orientation, although $\chi2$ is essentially eclipsed (~0°, which permits hydrogen bonding of the Asn side-chain atoms). Pro134 in the WT* structure exhibits average main-chain ϕ, ψ angles of −75° and 129°, respectively. In the Pro134Cys mutation the ϕ, ψ angles of position 134 exhibit average values of −93° and 107°, respectively. The substitution of Pro at position 134 is therefore associated with approximately 20° adjustments in both ϕ, and ψ main-chain angles, indicating the potential release of structural strain associated with the WT* Pro imino acid, although this appears to be a relatively modest adjustment and no substantial changes in inter-strand hydrogen bonding is observed. Analysis of refined thermal factors for main-chain atoms in the mutation X-ray structures compared to WT* shows no significant changes in response to the mutations. Overall, therefore, when taking into account β-sheet propensity changes, van der Waals interactions, evidence of structural strain, inter-strand hydrogen-bonding, and thermal factor changes, the observed increases in stability for mutations at positions 12, 95 and 134 appear unexpectedly large.

As described above, a major portion of the increased stability of the position 12, 95 and 134 mutations correlates with $\Delta\Delta G_F$, and this can be due to stabilization of the transition state and/or destabilization of the denatured state. However, if the denatured state energetics are unchanged then the observed $\Delta\Delta G$ is exclusively attributed to stabilization of the native state, and this is difficult to fully rationalize with the observed structural data. Several studies of mutational effects upon protein stability have proposed a significant contribution to overall ΔG from energetic changes in the denatured state; the majority of these describing a reduced entropy of unfolding.[20–22] Substitution of Lys12 and Asn95 by β-branched Val may reduce the entropy of the denatured state due to side-chain–backbone interactions unique to β-branched residues,[17,18] thus making a favorable contribution to overall ΔG. However, similar increases in stability are observed at position 12 with Cys mutations (a non-β-branched residue). Furthermore, at position 134 it is unclear how substitution of Pro by Val, Thr or Cys might decrease the entropy of the denatured state. We note that several mutants exhibit increased unfolding m values (Table 2), associated with

increased cooperativity of unfolding. These mutations may reflect an increase in net hydrophobic buried area that is critically contributing to native state stability. Further work is required to elucidate the basis of the substantial increase in stability for these mutations, and their potential for destabilizing the denatured state.

Following our long-standing interest in the consequences of primary structure symmetry within a symmetric superfold, the effects of Val mutations at symmetry-related positions to residues 12 and 134 were also examined. The ability of a symmetric tertiary structure to accommodate a symmetric primary structure has important implications for protein evolution and *de novo* design. Despite a ~1 Å root-mean-square deviation when comparing the backbone atoms of the three structurally related sub domains in FGF-1, the primary structure identity is marginally above random (Figure 1).[23–27] The symmetry mates of position Lys12 are Val54 and Asn95 (Figure 1). Position 54 is already a Val residue, and so mutation of positions 12 and 95 to Val constrain these three symmetry-related positions to Val. Although the Asn95Val mutation provides a substantial −6.4 kJ/mol increase in stability (Table 1), it has ~1000-fold reduction in mitogenic activity (Table 4). Analysis of the FGF receptor (FGFR)/FGF-1 complex (PDB accession code 1E0O) shows that Asn95 in FGF-1 makes an important hydrogen bonding interaction with Arg251 in the D2 and D3 linker of FGFR[28] and the observed lack of mitogenicity appears due to disruption of this key contact. Asn95 is highly conserved in the FGF family (Table 1), however, its role in receptor binding is achieved at significant thermodynamic expense; thus, providing further support to the "function/stability tradeoff" hypothesis of protein evolution.[29–33]

The Glu87Val mutation appears neutral in its effect upon stability (Table 1), but its mitogenicity is decreased by a factor of 3 (Table 4). Analysis of the FGFR–/FGF-1 complex shows that Glu87 in FGF-1 makes a hydrogen bonding interaction with Arg255 of the receptor. Disruption of this interaction has diminished the mitogenicity, but not to the extent observed for the Asn95Val mutation; thus, the Asn95/Arg251(FGFR) interaction appears to be of considerably greater importance in formation of the FGF-1/FGFR complex than the Glu87/Arg255 (FGFR) interaction. Glu87 is also highly conserved in the FGF family (Figure 1), but in this case, the receptor-binding function is accommodated with minimal penalty to protein stability.

The quintuple FGF-1 mutation (Lys12Val/Leu46-Val/Glu87Val/Asn95Val/Pro134Val) is the most stable in the series of mutations studied. The increase in stability ($\Delta\Delta G$) is −25.7 kJ/mol (Table 1); given that the overall stability of WT* FGF-1 (ΔG) is 21.0 kJ/mol (Table 1) the quintuple mutation has more than doubled this value. Previously reported FGF-1 symmetric constraint mutations have resulted in increases of −16.1 kJ/mol,[26] again, almost doubling the magnitude of ΔG for the WT* protein. Together, these results suggest that although FGF-1 is noted for its generally poor thermal stability,[34,35] the fundamental β-trefoil architecture appears capable of substantial thermal stability. It is known that the extensive functional diversity of the proteome is achieved by a surprisingly limited set of fundamental protein architectures.[36,37] The utility of the β-trefoil superfold is emphasized by the present results; if capable of extreme thermal stability, the functional radiation can be extensive even with a function/stability tradeoff. Given that the increase in stability was also accomplished with an increase in the 3-fold symmetric constraint upon the primary structure, the results also support the hypothesis that a symmetric primary structure within the symmetric β-trefoil tertiary structure is a solution and not a constraint to achieve a foldable polypeptide.[26] Thus, there is greater confidence that a symmetric *de novo* design principle can be successfully utilized for β-trefoil type proteins, and furthermore, that an evolutionary pathway of gene duplication and fusion in the emergence of this protein architecture is certainly within the realm of possibility.[38,39]

Mutations that stabilize FGF-1 can increase the effective mitogenic potency, presumably due to increased effective half-life.[26,40] Both Val mutations at positions 12 and 134 exhibit greater functional activity in comparison to WT*, with the Lys12Val mutation having the greatest increase in mitogenicity (Table 4). The Lys12 side-chain does not directly interact with FGFR (PDB accession code 1E0O), neither does Pro134. Thus, the basis for their differential mitogenic activity (given their near-identical stability increase) is unclear. Nonetheless, the Lys12Val/Pro134Val double mutation exhibits the greatest mitogenic activity, approximately 30 times more potent than WT*, and is −17.7 kJ/mol more stable than WT*. Such mutant forms of FGF-1 may find application as "second generation" forms of FGF-1 in angiogenic therapy for the treatment of ischemia.[3,41]

Sciences, Office of Science, under contract no. W-31-109-Eng-38.

Materials and Methods

Mutagenesis and expression

Mutation construction and expression followed described procedures.[24,35,42] Briefly, all studies utilized a synthetic gene for the 140 amino acid form of human FGF-1[23,43–45] with the addition of an amino-terminal six residue "His-tag" to facilitate purification.[24] Here a Cys117Val mutation form of FGF-1 was chosen as the reference protein for the current set of mutations, and is referred to as WT*. The Cys117Val mutation has minimal effects upon stability, folding or function of FGF-1[24] but eliminates a surface exposed cysteine residue that can form an intermolecular disulfide bond. The QuikChange™ site-directed mutagenesis protocol (Stratagene, La Jolla, CA) was used to introduce individual or combination mutations using mutagenic oligonucleotides of 25 to 31 bases in length (Biomolecular Analysis Synthesis and Sequencing Laboratory, Florida State University). All FGF-1 mutations

were expressed using the pET21a(+) plasmid/BL21(DE3) *Escherichia coli* host expression system (Invitrogen Corp., Carlsbad CA). Mutant proteins were purified as described[24] using nickel-nitrilotriacetic acid (Ni-NTA) chromatography followed by affinity purification using heparin Sepharose chromatography (G.E. Healthcare, Piscataway NJ). Sites for Cys mutations leading to potential disulfide bond formation were identified using the Disulfide by Design program[46] and the X-ray coordinates of wild-type FGF-1.[23]

Isothermal equilibrium denaturation

Isothermal equilibrium denaturation by GuHCl was quantified using fluorescence as the spectroscopic probe. FGF-1 contains a single buried tryptophan residue (Trp107) that exhibits greater fluorescence quenching in the native versus denatured state.[23,35] The differential fluorescence between the native and denatured state has been used to quantify the unfolding of FGF-1, in excellent agreement with unfolding as monitored by CD spectroscopy.[25,35] Fluorescence data were collected on a Varian Eclipse fluorescence spectrophotometer equipped with a Peltier controlled temperature regulator at 298K and using a 1 cm path-length cuvette. Protein samples (5 μM) were equilibrated overnight in ADA buffer (20 mM *N*-(2-acetamido)iminodiacetic acid (ADA), 100 mM NaCl, 2 mM DTT (pH 6.6) at 298K in 0.1 M increments of GuHCl. Triplicate scans were collected and averaged, and buffer traces were collected and subsequently subtracted from the protein scans. All scans were integrated to quantify the total fluorescence as a function of denaturant concentration. The general purpose non-linear least squares fitting program DataFit (Oakdale Engineering, Oakdale, PA) was used to fit the change in fluorescence *versus* GuHCl concentration data to a six parameter two-state model:[47]

$$F = \frac{F_{0N} + S_N[D] + (F_{0D} + (S_D[D]))e^{-(\Delta G_0 + m[D])/RT}}{1 + e^{-(\Delta G_0 + m[D])/RT}} \quad (1)$$

where $[D]$ is the denaturant concentration, F_{0N} and F_{0D} are the 0 M denaturant molar ellipticity intercepts for the native and denatured state baselines, respectively, and S_N and S_D are the slopes of the native and denatured state baselines, respectively. ΔG_0 and m describe the linear function of the unfolding free energy *versus* denaturant concentration. The effect of a given mutation upon the stability of the protein ($\Delta\Delta G$) was calculated by taking the difference between the C_m values for WT* and mutation proteins and multiplying by the average of the m values, as described by Pace and Scholtz:[48]

$$\Delta\Delta G = (C_{m\ WT*} - C_{m\ mutation})(m_{WT*} + m_{mutation})/2 \quad (2)$$

Folding kinetics measurements

Initial studies using manual mixing indicated that the relaxation times for folding were more appropriate for stopped-flow data collection. Denatured protein samples were prepared by overnight dialysis against ADA buffer containing either 2.5 M or 3.0 M GuHCl (depending upon the overall stability of the mutation). All folding kinetic data were collected using a KinTek SF2000 stopped-flow system (KinTek Corp., Austin TX). Folding was initiated by a 1:10 dilution of 40 μM denatured protein into ADA buffer with denaturant concentrations varying in increments of 0.05 M or 0.1 M, to the midpoint of denaturation as determined by the above described isothermal equilibrium denaturation measurements. The data collection strategy was designed to span approximately five half-lives, or >97% of the expected fluorescence signal change between the fully denatured and native states.

Unfolding kinetics measurements

Unfolding kinetics measurements were performed using a manual mixing technique. Protein samples (~30 μM) were dialyzed against ADA buffer overnight at 298K. Unfolding was initiated by a 1:10 dilution into ADA buffer with a final GuHCl concentration of 1.5 M to 5.5 M in 0.5 M increments. All unfolding data were collected using a Varian Eclipse fluorescence spectrophotometer equipped with a Peltier controlled temperature unit at 298K. Data collection times for each protein were designed so as to quantify the fluorescence signal over three to four half-lives, or >93% of the total expected amplitude.

Folding and unfolding kinetics analysis

The folding and unfolding characteristics of FGF-1 have been described in detail.[9] Briefly, the unfolding kinetic data exhibits an excellent fit to single exponential decay at all denaturant concentrations. The folding kinetic data also exhibits an excellent fit to a single exponential model, but only for denaturant concentrations above approximately 0.6 M GuHCl. Below this concentration, the folding kinetic data exhibits bi-exponential properties; with the slow phase being generally independent of denaturant concentration. The fast phase of this bi-exponential folding regime lies on the extrapolated region of the single-exponential folding data. Thus, the folding constant is derived from a fit to the mono-exponential region and the fast phase of the bi-exponential region. The ΔG values derived from the folding and unfolding kinetic data are in excellent agreement with the values obtained from isothermal equilibrium denaturation data, as well as differential scanning calorimetry.[9]

Both folding and unfolding kinetic data were collected in triplicate at each GuHCl concentration; data from at least three separate experiments were averaged in each case. The kinetic rates and amplitudes *versus* denaturant concentration were calculated from the time dependent change in tryptophan fluorescence using a single exponential model:

$$I(t) = A\exp(-kt) + C \quad (3)$$

where $I(t)$ is the intensity of fluorescent signal at time t, A is the corresponding amplitude, k is the observed rate constant for the reaction and C is the asymptote of the fluorescence signal. Folding and unfolding rate constant data were fit to a global function describing the contribution of both rate constants to the observed kinetics as a function of denaturant (chevron plot) as described by Fersht:[49]

$$\ln(k_{obs}) = \ln(k_{f0}\exp(m_f[D]) + k_{u0}\exp(m_u[D])) \quad (4)$$

where k_{f0} and k_{u0} are the folding and unfolding rate constants, respectively, extrapolated to 0 M denaturant, m_f and m_u are the slopes of the linear functions relating $\ln(k_f)$ and $\ln(k_u)$, respectively, to denaturant concentration, and $[D]$ is the denaturant concentration.

The concentration of denaturant at the midpoint of denaturation (C_m) was determined from the folding and unfolding rate constants and *m*-values:

$$C_m = (\ln k_f - \ln k_u)/(m_u - m_f) \quad (5)$$

The linear dependence of ΔG of unfolding as a function of denaturant (*m*-value) was determined from the kinetic m_u and m_f values:

$$m\text{-value} = (m_u - m_f)*RT \quad (6)$$

The mutational effect upon protein stability ($\Delta\Delta G$) was determined from the kinetic data using the derived WT* and mutation C_m values (equation (5)) and *m*-values (equation (6)) and the method of Pace and Scholtz[48] (equation (2)).

The mutational change in the free energy barrier to folding in the reaction coordinate from denatured to the transition state ($\Delta\Delta G_F$), and from native to the transition state ($\Delta\Delta G_U$) were calculated from the WT* and mutation folding and unfolding kinetic constants:

$$\Delta\Delta G_F = RT*\ln(k_{f\ WT*}/k_{f\ mut}) \quad (7)$$

$$\Delta\Delta G_U = RT*\ln(k_{u\ WT*}/k_{u\ mut}) \quad (8)$$

β_T values, which provide information on the solvent accessible surface area of the transition state, were calculated from the folding and unfolding *m*-values according to Jackson:[10]

$$\beta_T = -m_f/(m_u - m_f) \quad (9)$$

Crystallization of FGF-1 mutations, X-ray data collection, refinement and cavity calculations

Purified protein for crystallization trials was dialyzed against crystallization buffer (50 mM sodium phosphate, 100 mM NaCl, 10 mM ammonium sulfate, 2 mM DTT (pH 7.5)) and concentrated to 10–16 mg/ml. Crystals were grown at room temperature using the hanging-drop vapor diffusion method with 7 μl drop size and 1 ml of reservoir solution. Diffraction quality crystals grew from reservoirs containing 3.2–4.3 M sodium formate and 0.25–0.5 M ammonium sulfate, with the exception of the Pro134Cys mutation which grew from 3.6 M sodium formate with no added ammonium sulfate.

Diffraction data for all mutations except Pro134Cys, was collected at the Southeast Regional Collaborative Access Team (SER-CAT) 22-BM beam line (λ = 1.00 Å) at the Advanced Photon Source, Argonne National Laboratory, using a MarCCD225 detector (Mar USA, Evanston, IL). Pro134Cys mutation diffraction data were collected using an in-house Rigaku RU-H2R copper rotating anode (λ = 1.54 Å) X-ray generator (Rigaku MSC, The Woodlands, TX) coupled to an Osmic Purple confocal mirror system (Osmic, Auburn Hills, MI) and a MarCCD165 detector (Mar USA, Evanston, IL). In all cases, crystals were mounted and maintained in a stream of gaseous nitrogen at 100 K. Diffraction data were indexed, integrated and scaled using the HKL2000 software.[50,51] His-tagged wild-type FGF-1 (PDB code 1JQZ) was used as the search model in molecular replacement using the CNS software suite.[52] Model building and visualization utilized the O molecular graphics program.[53] Structure refinement utilized the CNS software suite, with 5% of the data in the reflection files set aside for R_{free} calculations.[54] Quantification of solvent-excluded cavities with the refined mutation structures was performed using the MSP software package.[55]

Mitogenic assay

The mitogenic activity of certain mutations was evaluated by a cultured fibroblast proliferation assay. NIH 3T3 fibroblasts were initially plated in Dulbecco's modified Eagle's medium (DMEM) (American Type Culture Collection, Manassas VA) supplemented with 10% (v/v) newborn calf serum (NCS) (Sigma, St Louis MO), 100 units of penicillin, 100 mg of streptomycin, 0.25 mg of Fungizone™ and 0.01 mg/ml of gentamicin (Gibco, Carlsbad CA) (serum-rich medium) in T75 tissue culture flasks (Fisher, Pittsburgh PA). The cultures were incubated at 37 °C with 5%(v/v) CO_2 supplementation. At 80% cell confluence, the cells were washed with 5 ml of cold TBS (0.14 M NaCl, 5.1 mM KCl, 0.7 mM Na_2HPO_4, 24.8 mM Trizma base (pH 7.4)) and subsequently treated with 5 ml of a 0.025%(v/v) trypsin solution (Invitrogen Corp., Carlsbad CA). The trypsinized cells were subsequently seeded in T25 tissue culture flasks at a density of 3.0×10^4 cells/cm^2 (representing 20% confluence). Cell synchronization was initiated by serum starvation in DMEM with 0.5% NCS, 100 units of penicillin, 100 mg of streptomycin, 0.25 mg of Fungizone™ and 0.01 mg/ml of gentamicin (starvation medium). Cultures were incubated for 48 h at 37 °C, the medium was then decanted and replaced with fresh medium supplemented with FGF-1 (0–10 μg/ml), and the cultures incubated for an additional 48 h. After this incubation, the medium was decanted and the cells were washed with 1 ml of cold TBS.Then 1 ml of 0.025% trypsin was then added to release the cells from the flask surface, and 2 ml of serum-rich medium was added to dilute and inhibit the trypsin. The cells were counted using a hemacytometer (Hausser Scientific Partnership, Horsham PA). Experiments were performed in quadruplicate and the cell densities were averaged. The relationship between the cell number and log concentration of added growth factor was fit to a sigmoid function. The midpoint of the fitted sigmoid function represents the concentration of added growth factor necessary to achieve 50% stimulation (EC_{50} value), and is used for quantitative comparison of mitogenicity.

Protein Data Bank accession codes

All X-ray structures have been deposited in the RCSB Protein Data Bank (PDB) under the accession codes provided in Table 3.

Acknowledgements

We thank Dr Claudius Mundoma Physical Biochemistry Facility, Kasha Laboratory, Institute of Molecular Biophysics for his valuable suggestions. We also thank Ms Pushparani Dhanarajan, Molecular Cloning Facility, Biological Science for helpful comments. We acknowledge the instrumentation facilities at Biomedical Proteomics Laboratory, College of Medicine. This work was supported by grant MCB 0314740 from the National Science Foundation and grant 0655133B from the American

Heart Association. Use of "mail-in crystallography" facility of SER-CAT for diffraction data collection is acknowledged. Use of the Advanced Photon Source was supported by the US Department of Energy, Basic Energy.

References

1. Folkman, J. (1982). Angiogenesis: initiation and control. *Annal. NY Acad. Sci.* **401**, 212–227.
2. Thomas, K. A., Rios-Candelore, M., Gimenez-Gallego, G., DiSalvo, J., Bennett, C., Rodkey, J. & Fitzpatrick, S. (1985). Pure brain-derived acidic fibroblast growth factor is a potent angiogenic vascular endothelial cell mitogen with sequence homology to interleukin 1. *Proc. Natl Acad. Sci. USA*, **82**, 6409–6413.
3. Stegmann, T. J., Hoppert, T., Schneider, A., Popp, M., Strupp, G., Ibing, R. O. & Hertel, A. (2000). Therapeutic angiogenesis: intramyocardial growth factor delivery of FGF-1 as sole therapy in patients with chronic coronary artery disease. *Cardiac. Vasc. Regen.* **1**, 259–267.
4. McLachlan, A. D. (1979). Three-fold structural pattern in the soybean trypsin inhibitor (Kunitz). *J. Mol. Biol.* **133**, 557–563.
5. Murzin, A. G., Lesk, A. M. & Chothia, C. (1992). β-Trefoil fold. Patterns of structure and sequence in the kunitz inhibitors interleukins-1β and 1α and fibroblast growth factors. *Jour. J. Mol. Biol.* **223**, 531–543.
6. Samuel, D., Kumar, T. K. S., Balamurugan, K., Lin, W.-Y., Chin, D.-H. & Yu, C. (2001). Structural events during the refolding of an all β-sheet protein. *J. Biol. Chem.* **276**, 4134–4141.
7. Bernett, M. J., Somasundaram, T. & Blaber, M. (2004). An atomic resolution structure for human fibroblast growth factor 1. *Proteins: Struct. Funct. Genet.* **57**, 626–634.
8. Lozano, R. M., Pineda-Lucena, A., Gonzalez, C., Angeles Jimenez, M., Cuevas, P., Redondo-Horcajo, M. *et al.* (2000). ^{1}H NMR structural characterization of a nonmitogenic, vasodilatory, ischemia-protector and neuromodulatory acidic fibroblast growth factor. *Biochemistry*, **39**, 4982–4993.
9. Kim, J., Brych, S. R., Lee, J., Logan, T. M. & Blaber, M. (2003). Identification of a key structural element for protein folding within β-hairpin turns. *J. Mol. Biol.* **328**, 951–961.
10. Jackson, S. (1998). How do small single-domain proteins fold? *Fold. Design*, **3**, R81–R91.
11. Eriksson, A. E., Baase, W. A., Zhang, X.-J., Heinz, D. W., Blaber, M., Baldwin, E. P. & Matthews, B. W. (1992). Response of a protein structure to cavity-creating mutations and its relation to the hydrophobic effect. *Science*, **255**, 178–183.
12. Kim, C. A. & Berg, J. M. (1993). Thermodynamic beta-sheet propensities measured using a zinc-finger host peptide. *Nature*, **362**, 267–270.
13. Minor, D. L. J. & Kim, P. S. (1994). Measurement of the b-sheet-forming propensities of amino acids. *Nature*, **367**, 660–663.
14. Minor, D. L., Jr & Kim, P. S. (1994). Context is a major determinant of beta-sheet propensity. *Nature*, **371**, 264–267.
15. Smith, C. K., Withka, J. M. & Regan, L. (1994). A thermodynamic scale for the beta-sheet forming tendencies of the amino acids. *Biochemistry*, **33**, 5510–5517.
16. Otzen, D. E. & Fersht, A. R. (1995). Side-chain determinants of beta-sheet stability. *Biochemistry*, **34**, 5718–5724.
17. Street, A. G. & Mayo, S. L. (1999). Intrinsic beta-sheet propensities result from van der Waals interactions between side chains and the local backbone. *Proc. Natl Acad. Sci. USA*, **96**, 9074–9076.
18. Pal, D. & Chakrabarti, P. (2000). beta-sheet propensity and its correlation with parameters based on conformation. *Acta Crystallog. sect. D*, **56**, 589–594.
19. Zaremba, S. M. & Gregoret, L. M. (1999). Context-dependence of amino acid residue pairing in antiparallel beta-sheets. *J. Mol. Biol.* **291**, 463–479.
20. Chakraborty, K., Thakurela, S., Prajapati, R. S., Indu, S., Ali, P. S., Ramakrishanan, C. & Varadarajan, R. (2005). Protein stabilization by introduction of cross-strand disulfides. *Biochemistry*, **44**, 14638–14646.
21. Chaudhuri, T. K., Horii, K., Yoda, T., Arai, M., Nagata, S., Terada, T. P. *et al.* (1999). Effect of the extra N-terminal methionine residue on the stability and folding of recombinant alpha-lactalbumin expressed in *Escherichia coli*. *J. Mol. Biol.* **285**, 1179–1194.
22. Matthews, B., Nicholson, H. & Becktel, W. (1987). Enhanced protein thermostability from site-directed mutations that decrease the entropy of unfolding. *Proc. Natl Acad. Sci. USA*, **84**, 6663–6667.
23. Blaber, M., DiSalvo, J. & Thomas, K. A. (1996). X-ray crystal structure of human acidic fibroblast growth factor. *Biochemistry*, **35**, 2086–2094.
24. Brych, S. R., Blaber, S. I., Logan, T. M. & Blaber, M. (2001). Structure and stability effects of mutations designed to increase the primary sequence symmetry within the core region of a β-trefoil. *Protein Sci.* **10**, 2587–2599.
25. Brych, S. R., Kim, J., Logan, T. M. & Blaber, M. (2003). Accommodation of a highly symmetric core within a symmetric protein superfold. *Protein Sci.* **12**, 2704–2718.
26. Brych, S. R., Dubey, V. K., Bienkiewicz, E., Lee, J., Logan, T. M. & Blaber, M. (2004). Symmetric primary and tertiary structure mutations within a symmetric superfold: a solution, and not a constraint, to achieve a foldable polypeptide. *J. Mol. Biol.* **344**, 769–780.
27. Dubey, V. K., Lee, J. & Blaber, M. (2005). Redesigning symmetry-related "mini-core" regions of FGF-1 to increase primary structure symmetry: thermodynamic and functional consequences of structural symmetry. *Protein Sci.* **14**, 2315–2323.
28. Plotnikov, A. N., Schlessinger, J., Hubbard, S. R. & Mohammadi, M. (1999). Structural basis for FGF receptor dimerization and activation. *Cell*, **98**, 641–650.
29. Schreiber, G., Buckle, A. M. & Fersht, A. R. (1994). Stability and function: two constraints in the evolution of barstar and other proteins. *Structure*, **2**, 945–951.
30. Shoichet, B. K., Baase, W. A., Kuroki, R. & Matthews, B. W. (1995). A relationship between protein stability and protein function. *Proc. Natl Acad. Sci. USA*, **92**, 452–456.
31. Wang, X., Minasov, G. & Shoichet, B. K. (2002). Evolution of an antibiotic resistance enzyme constrained by stability and activity trade-offs. *J. Mol. Biol.* **320**, 85–95.
32. Bloom, J. D., Wilke, C. O., Arnold, F. H. & Adami, C. (2004). Stability and the evolvability of function in a model protein. *Biophys. J.* **86**, 2758–2764.
33. Jager, M., Zhang, Y., Bieschke, J., Nguyen, H., Dendle, M., Bowman, M. E. *et al.* (2006). Structure-function-folding relationship in a WW domain. *Proc. Natl Acad. Sci. USA*, **103**, 10648–10653.
34. Copeland, R. A., Ji, H., Halfpenny, A. J., Williams, R. W., Thompson, K. C., Herber, W. K. *et al.* (1991). The structure of human acidic fibroblast growth factor and

its interaction with heparin. *Arch. Biochem. Biophys.* **289**, 53–61.
35. Blaber, S. I., Culajay, J. F., Khurana, A. & Blaber, M. (1999). Reversible thermal denaturation of human FGF-1 induced by low concentrations of guanidine hydrochloride. *Biophys. J.* **77**, 470–477.
36. Orengo, C. A., Jones, D. T. & Thornton, J. M. (1994). Protein superfamilies and domain superfolds. *Nature*, **372**, 631–634.
37. Thornton, J. M., Orengo, C. A., Todd, A. E. & Pearl, F. M. (1999). Protein folds, functions and evolution. *J. Mol. Biol.* **293**, 333–342.
38. Mukhopadhyay, D. (2000). The molecular evolutionary history of a winged bean α-chymotrypsin inhibitor and modeling of its mutations through structural analysis. *J. Mol. Evol.* **50**, 223–314.
39. Ponting, C. P. & Russell, R. B. (2000). Identification of distant homologues of fibroblast growth factors suggests a common ancestor for all beta-trefoil proteins. *J. Mol. Biol.* **302**, 1041–1047.
40. Arakawa, T., Horan, T. P., Narhi, L. O., Rees, D. C., Schiffer, S. G., Holst, P. L. *et al.* (1993). Production and characterization of an analog of acidic fibroblast growth factor with enhanced stability and biological activity. *Protein Eng.* **6**, 541–546.
41. Thompson, J. A., Haudenschild, C. C., Anderson, K. D., DiPietro, J. M., Anderson, W. F. & Maciag, T. (1989). Heparin-binding growth factor 1 induces the formation of organoid neovascular structures *in vivo*. *Proc. Natl Acad. Sci. USA*, **86**, 7928–7932.
42. Culajay, J. F., Blaber, S. I., Khurana, A. & Blaber, M. (2000). Thermodynamic characterization of mutations of human fibroblast growth factor 1 with an increased physiological half-life. *Biochemistry*, **39**, 7153–7158.
43. Gimenez-Gallego, G., Conn, G., Hatcher, V. B. & Thomas, K. A. (1986). The complete amino acid sequence of human brain-derived acidic fibroblast growth factor. *Biochem. Biophys. Res. Commun.* **128**, 611–617.
44. Linemeyer, D. L., Menke, J. G., Kelly, L. J., Disalvo, J., Soderman, D., Schaeffer, M.-T. *et al.* (1990). Disulfide bonds are neither required, present, nor compatible with full activity of human recombinant acidic fibroblast growth factor. *Growth Factors*, **3**, 287–298.
45. Ortega, S., Schaeffer, M.-T., Soderman, D., DiSalvo, J., Linemeyer, D. L., Gimenez-Gallego, G. & Thomas, K. A. (1991). Conversion of cysteine to serine residues alters the activity, stability, and heparin dependence of acidic fibroblast growth factor. *J. Biol. Chem.* **266**, 5842–5846.
46. Dombkowski, A. A. (2003). Disulfide by Design: a computational method for the rational design of disulfide bonds in proteins. *Bioinformatics*, **19**, 1852–1853.
47. Eftink, M. R. (1994). The use of fluorescence methods to monitor unfolding transitions in proteins. *Biophys. J.* **66**, 482–501.
48. Pace, C. N. & Scholtz, J. M. (1997). Measuring the conformational stability of a protein. In *Protein Structure: A Practical Approach* (Creighton, T. E., ed), pp. 299–321, Oxford University Press, Oxford.
49. Fersht, A. R. (1999). *Kinetics of Protein Folding. Structures and Mechanism in Protein Science.* W.H. Freeman and Co., New York.
50. Otwinowski, Z. (1993). *Data Collection and Processing. Proceedings of the CCP4 Study Weekend.* Warrington, UK.
51. Otwinowski, Z. & Minor, W. (1997). Processing of X-ray diffraction data collected in oscillation mode. *Methods Enzymol.* **276**, 307–326.
52. Brunger, A. T., Adams, P. D., Clore, G. M., DeLano, W. L., Gros, P., Grosse-Kunstleve, R. W. *et al.* (1998). Crystallography and NMR system (CNS): a new software system for macromolecular structure determination. *Acta Crystallog. sect. D*, **54**, 905–921.
53. Jones, T. A., Zou, J. Y., Cowan, S. W. & Kjeldgaard, M. (1991). Improved methods for the building of protein models in electron density maps and the location of errors in these models. *Acta Crystallog. sect. A*, **47**, 110–119.
54. Brunger, A. T. (1992). Free *R* value: a novel statistical quantity for assessing the accuracy of crystal structures. *Nature*, **355**, 472–475.
55. Connolly, M. L. (1993). The molecular surface package. *J. Mol. Graph.* **11**, 139–141.

Edited by F. Schmid

(Received 13 November 2006; received in revised form 22 April 2007; accepted 21 May 2007)
Available online 31 May 2007